Machine Learning Prediction of Elastic Properties and Glass Forming Ability of Bulk Metallic Glasses

Jie Xiong[b], Tong-Yi Zhang[a*] and San-Qiang Shi[b*]

[a]Material Genome Institute, Shanghai University, Shanghai, China; [b]Department of Mechanical Engineering, The Hong Kong Polytechnic University, Hong Kong, China

ABSTRACT: There is a genuine need to shorten the development period for new materials with desired properties. In this work, Machine Learning (ML) was conducted on a dataset of 219 bulk metallic glasses (BMGs) with the elastic moduli and another dataset of 630 BMGs with the critical casting diameters ($D_{\max}$). The predicted moduli and D_{max} with the ML model were in good agreement with most experimentally measured ones and the models have identified some errors reported in the literature. This work indicates the great potential of ML in advanced materials design with target properties.

Keywords: Material Informatics; metallic glasses; machine learning.

Introduction

Bulk metallic glasses (BMGs), as promising materials with unique structural features and outstanding mechanical, physical and chemical properties [1], have been extensively studied, because of their potential applications in various fields, since they were first discovered in 1960 by Duwez and co-workers [2]. However, the relationship between mechanical property and chemical composition in BMGs has not been established due to the poor understanding of the underlying physics [3,4]. At the moment, it is difficult to develop an analytic model to design a new BMG with targeted properties. As a result, it requires a long time to discover and optimize a potential material for application via the traditional paradigm of materials science and engineering [5].

Along with the fast development of artificial intelligence, the paradigm of "machine learning" or "materials informatics", which unifies the knowledge learned from experiments, theory, computations and simulations, is rapidly becoming popular in the field of materials science [3-8]. Integrating artificial intelligence with materials science and engineering may accelerate the design and discovery of advanced materials. A few groups of researchers have employed machine learning to study metallic glasses. In 2017, Sun and co-workers employed support vector machine to study the glass-forming-ability (GFA) of binary metallic alloys with random compositions [8]. Ward and Ren applied the machine learning approach on metallic glasses containing three or more elements in 2018 [9,10]. Their findings suggest that Machine learning (ML) has the great potential to discover new metallic glasses with good GFA.

The present work uses ML to study BMG with the aim to predict elastic moduli (bulk modulus K and shear modulus G). A four-step procedure is used in this study: (1) Data collection: the sets of experimental data on metal-metal BMGs was collected from the literature; (2) Feature selection: the best subset-selection (BSS) algorithm was applied to select the best features from feature candidates; (3) Parameter tuning: the parameter of ML model was tunning by opimazation technique; (4) ML model validation: the machinle learning model was trained and tested by leave-one-out cross-validation (LOOCV).

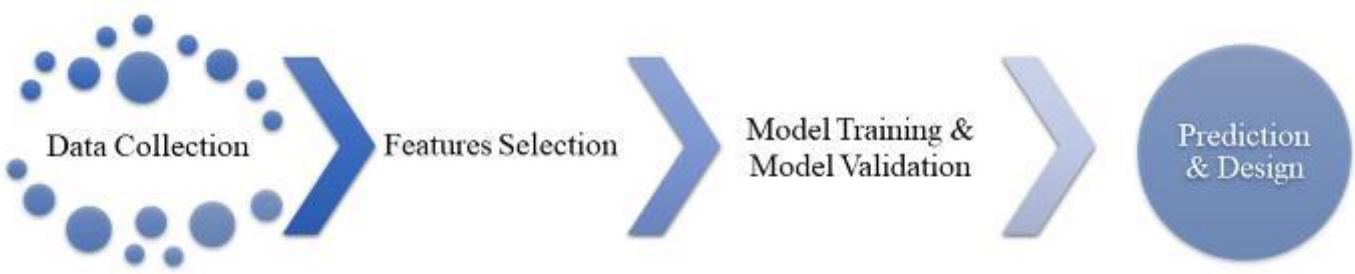

Figure 1. Four-step procedure used in this study: (1) Data collection; (2) Feature selection; (3) Parameter tuning; (4) ML validation.

Data Collection

We have built two training sets in this paper: (1) Elastic modulus dataset and (2) Critical casting diameter dataset.

Elastic modulus dataset: The shear modulus and bulk modulus for 219 metal-metal BMGs have been collected in this research. The 219 alloys are from 4 Ca-based, 23 Cu-based, 4 Hf-based, 69 LT-based (LT= Ce, Dy, Er, Gd, Ho, La, Lu, Nd, Pr, Sm, Tb, Tm and Yb), 21 Mg-based, 8 Ni-based, 1 Sc-based, 5 Sr-based, 4 Ti-Based, 78 Zr-based and 2 High-entropy alloys. All compositions herein are expressed in atomic fraction. And the elastic moduli were measured via ultrasonic-wave-propagation (UWP) methods

Critical casting diameter dataset: this set contains the characteristic temperatures and D_{max} for 442 metal-metal BMGs. The 442 alloys are from 19 Ag-based, 57 Ca-based, 84 Cu-based, 3 Hf-based, 111 LT-based, 60 Mg-based, 13 Ni-based, 1 Sc-based, 20 Ti-Based, 4 Y-based and 70 Zr-based alloys. All compositions herein are expressed in atomic fraction. Because of the fact that D_{max} can be affected by the fabrication method, only values obtained by copper mold casting method were chosen. And the most characteristic temperatures were measured by the differential thermal analysis and differential scanning calorimetry at a heating rate of 20 K/min.

Data standardization

The feature standardization method [16] was used to standardize the features, given by

$$x' = \frac{x - \bar{x}}{\sigma_x}$$

where $\bar{x}$ is the average feature value, and σ_x is the standard deviation.

Support vector regression (SVR) model

The WEKA software was used to build a SVR model. SVR is equipped with the kernel function which is used to covert the features into a higher dimensional space. With the kernel trick, the output ***y*** from any set of features ***x*** has a linear correlation at the higher space.

$$f(x) = < w, K(x) > + b$$

in which, *K(x)* is the kernel function, *w* and *b* are determined by $\operatorname{argmin}(\frac{1}{2}\|w\|^2 + C\sum_{i=1}^{m} L(f(x_i, y_i))$. *C* is the penalization parameter and *L* is the loss function: $L\big(f(x_i, y_i)\big) = \max\{|f(x_i) - y_i|\}$

Two kernel functions were used in this research, radial basis function (RBF) kernel and Pearson VII Universal Kernel (PUK)

RBF: $K(x_i, x_j) = \exp\left(-\gamma\|x_i - x_j\|^2\right)$

PUK: $K(x_i, x_j) = \left[1 + \left(\frac{\sqrt{\|x_i - x_j\|^2}\sqrt{2^{1/\omega} - 1}}{\sigma}\right)^2\right]^{-\omega}$

The RBF parameter γ, PUK parameters ω and σ were tuning via the grid search (GS) technique in this research, as well as parameter *C*.

Gaussian process (GP) model

The Matlab 2018 software was used to build the GP model. A GP model is characterized such that the output ***y*** from any set of features ***x*** has a multivariate normal distribution:

$$y = f(x)^T W + \varepsilon$$

where *W* is a constant vector, *f(x)* and ε are gaussian distribution, the probability density (PD) of these two distributions are:

$$\varepsilon \sim \mathcal{N}(0, \sigma),\ \mathrm{PD}(\varepsilon) = \frac{1}{\sigma_n\sqrt{2\pi}}\exp\left(-\frac{x^2}{2{\sigma_n}^2}\right)$$

$$f(x) \sim \mathcal{N}(0, K_f),\ \mathrm{PD}(f(x)) = \frac{1}{K_f\sqrt{2\pi}}\exp\left(-\frac{x^2}{2{K_f}^2}\right)$$

in which K_f is the covariance function, and the exponential function (EF) was used in this research

$$K_f = \sigma_f^2 \exp\left(-\frac{\|x_i - x_j\|}{\sigma_l}\right)$$

The σ_n, σ_f and σ_l were estimated via Matlab automatically.

Results and Discussion

Elastic modulus model

Selection of best-performance features

The bulk modulus is fundamentally related to the atomic bonding energy [10,11], which is influenced by the electronegativity (*EN*). The bulk modulus depends on the average atomic volume (V_A) [12], and the atomic size difference (δ) affects the ratio of *K* to *G* in metallic glasses [13]. There exists correlation among the critical cooling rate, elastic modulus and mixing entropy (S_m) [14]. Thus, the feature candidates in the present work include relative electronegativity (*REN*), absolute electronegativity (*AEN*), average atomic volume (V_A), atomic size difference (δ), and mixing entropy (S_m), which are defined by

$$REN = \sum a_i \, (EN_i - EN_o)$$

$$AEN = \sum a_i \, EN_i$$

$$V_A = \sum a_i \cdot \frac{4}{3}\pi r_i^3$$

$$\delta = \sqrt{\sum a_i \left(1 - \frac{r_i}{\bar{r}_i}\right)^2}$$

$$\mathrm{Sm} = -R \sum_{i=1}^{n} a_i ln \, \phi_i$$

where a_i is the atomic percentage of the i-th constituent, EN_o is the Pauling electronegativity of the major element in a BMG, r_i is the atomic radius and $\bar{r}_i$ is the average value. *R* is the ideal gas constant, ϕ_i is the volume percentages of *i*-th component. The replacement of a_i by ϕ_i in the logarithmic term of $S_{m\text{-}p}$ is due to the effect of dissimilar size of atoms [15].

Due to the poor understanding of metallic glasses, three types of atomic radius are considered here. The metallic radius (*rm*), the covalent atomic radius (*rc*) and the statistical radius. Their values are shown in Table 1 and the datasets containing all features shown in Table 2 will be used to train ML models.

Metallic radius [17] which is taken as half of the interatomic distance in the metallic lattice was widely used in studies of metallic glasses as the atomic radius [8,17,18]. This radius depends on the nature of the atom, as well as on the coordination number (*CN*). The metallic radius of an element in this work is calculated with a coordination number of 12 for closed packed lattice.

PENG et. al [19] used the covalent atomic radius to study the Mg-based metal-metal BMGs, and Lu et. al [20] also studied the Zr-based metal-metal BMGs with this radius. The covalent radius of Mg and Zr are calculated with a coordination number of 2 and 4, respectively [21]. The coordination numbers used in this work are shown in table 1.

The above two types of atomic radius use a constant coordination number. However, the structures of BMGs are known as the disordered structures, the atoms of same element might have different coordination numbers [22]. Thus, the statistical radius [23], which is the atomic radius based on a statistical analysis of more than 228,000 experimental bond length form the Cambridge Structure Database, was employed in this research.

The best subset selection (BSS) method [24] was applied to screen these feature candidates. If there are *m* feature candidates, the linear least-square regression (LLS) was used to fit for each possible combination of these feature candidates. That is to say, *m* LLS models are built that only include one feature candidate, $m(m-1)/2$ LLS models containing two feature candidates, and so forth [25].

Table 1 Data of electronegativity [26] and atomic radius [17,19,22] of elements.

Symbol	*EN*	*rm*		*rc*		*rs*	*Symbol*	*EN*	*rm*		*rc*		*rs*
		Value	*CN*	*Value*	*CN*				*Value*	*CN*	*Value*	*CN*	
Ag	1.93	144	12	128	1	145	***Mo***	2.16	139	12	138	6	154
Al	1.61	143	12	125	3	121	***Nb***	1.60	146	12	147	5	164
Au	2.54	144	12	124	1	136	***Nd***	1.14	181.4	12	174	3,6	201
Be	1.57	112	12	102	2	96	***Ni***	1.91	124	12	110	2	124
Ca	1.00	197	12	171	2	176	***Pb***	1.87	180	12	144	4	146
Ce	1.12	181.8	12	163	4	204	***Pd***	2.20	137	12	120	2	139
Co	1.88	125	12	111	3	126	***Pr***	1.13	182.4	12	176	5	203
Cr	1.66	128	12	122	6	139	***Pt***	2.28	138.5	12	123	2	136
Cu	1.90	128	12	112	1	132	***Sc***	1.36	162	12	148	3	170
Dy	1.22	178.1	12	167	3	192	***Sm***	1.17	180.4	12	172	3	198
Er	1.24	176.1	12	165	3	189	***Sn***	1.96	145	12	140	4	139
Fe	1.83	126	12	116	4	132	***Sr***	0.90	215	12	185	2	195
Gd	1.20	180.4	12	169	3	196	***Ta***	1.50	146	12	146	5	170
Ge	2.01	125	12	121	4	120	***Tb***	1.10	177.3	12	168	3	194
Hf	1.30	159	12	152	4	175	***Ti***	1.62	147	12	136	4	160
Ho	1.23	176.2	12	166	3	192	***Tm***	1.25	175.9	12	164	3	190

In	1.78	167	12	142	3	142	***V***	1.63	134	12	134	134	153
La	1.10	187	12	180	3	207	***Y***	1.22	180	12	163	3	190
Li	0.98	152	12	133	1	128	***Yb***	1.10	176	12	170	3	187
Lu	1.27	173.8	12	162	3	187	***Zn***	1.65	134	12	118	2	122
Mg	1.31	160	12	139	2	141	***Zr***	1.33	160	12	154	4	175
Mn	1.55	127	12	119	5	139							

Table 2. List of original datasets

Atomic radius	Target modulus	
	G	K
rm	GM	KM
rc	GC	KC
rs	GS	KS

The qualities of strained LLS models were tested by the LOOCV with the cross-validation root mean square error (*RMSE*), For a dataset containing *n* samples, a model was trained with *n*-1 training observations and the trained model was used to predict the target property $\hat{y}_i$ of remain observation, the root square error between the authentic value y_i and this predicted value are computed. Repeating this approach n times produces n root square errors, the average of these errors is cross-validation root mean square error (*RMSE*) is given by

$$RMSE = \sqrt{\sum_{i=1}^{n} \frac{1}{n} (\hat{y}_i - y_i)^2}$$

The BSS method selects the best LLS model, shown in Figure 2a for G and in Figure 2b for K. The best subset of features in GM is (*AEN*, V_A, S_m); in GC is (*REN*, *AEN*, V_A, δ, S_m); in GS is (*AEN*, V_A, δ), in KM and KC is (*AEN*, V_A, δ, S_m), and in KS is (*AEN*, V_A, δ). These best subsets are marked and used hereafter as TGs (TGM, TGC and TGS), and TKs (TKM, TKC and TKS).

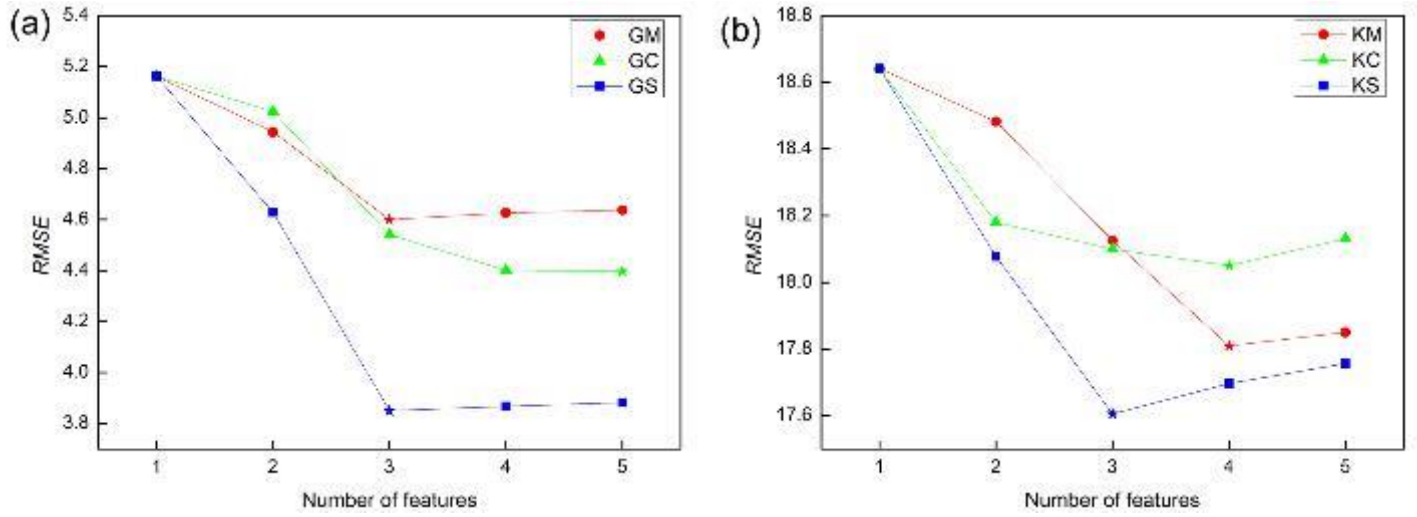

Figure 2. The cross-validation root mean square error of the best LLS model containing a subset of 1~5 features in training set for (a) *G* and (b) *K*.

Selection of the best type of atomic radius

Support vector regression (SVR) with a radial basis function (RBF) kernel [27,28] which shows much better performance than other algorithms (decision tree, gaussian process and so on) was used to develop ML models containing these eight selected subsets. Two SVR parameters [29], C (Penalty parameter) and γ (kernel parameter), were adjusted to strain the SVR model. Grid searches were conducted to obtain the best SVR-RBF model for each training set based on the correlation coefficient (*R*),

$$R = \sqrt{\frac{\sum_{i=1}^{n}(\hat{y}_i - \bar{y})^2}{\sum_{i=1}^{n}(y_i - \bar{y})^2}}$$

where $\bar{y}$ is the average of y_i, the *R* value lies between 0 and 1, with 1 indicating perfect fitting. The *R* values with different SVR-RBF parameters on TGs and TKs are shown in Figure 3(a-c) and 4(a-c), and the maximum values of *R* are marked with the green check. For comparison, Figures 3d and 4d plot the predicted values against the measured values [30] for *G* and *K*, respectively, with the best trained parameters of the SVR-RBF models.

It is clearly that the statistical radius performs much better than metallic radius and covalent radius. This radius is the best type of atomic radius to be used in ML procedure.

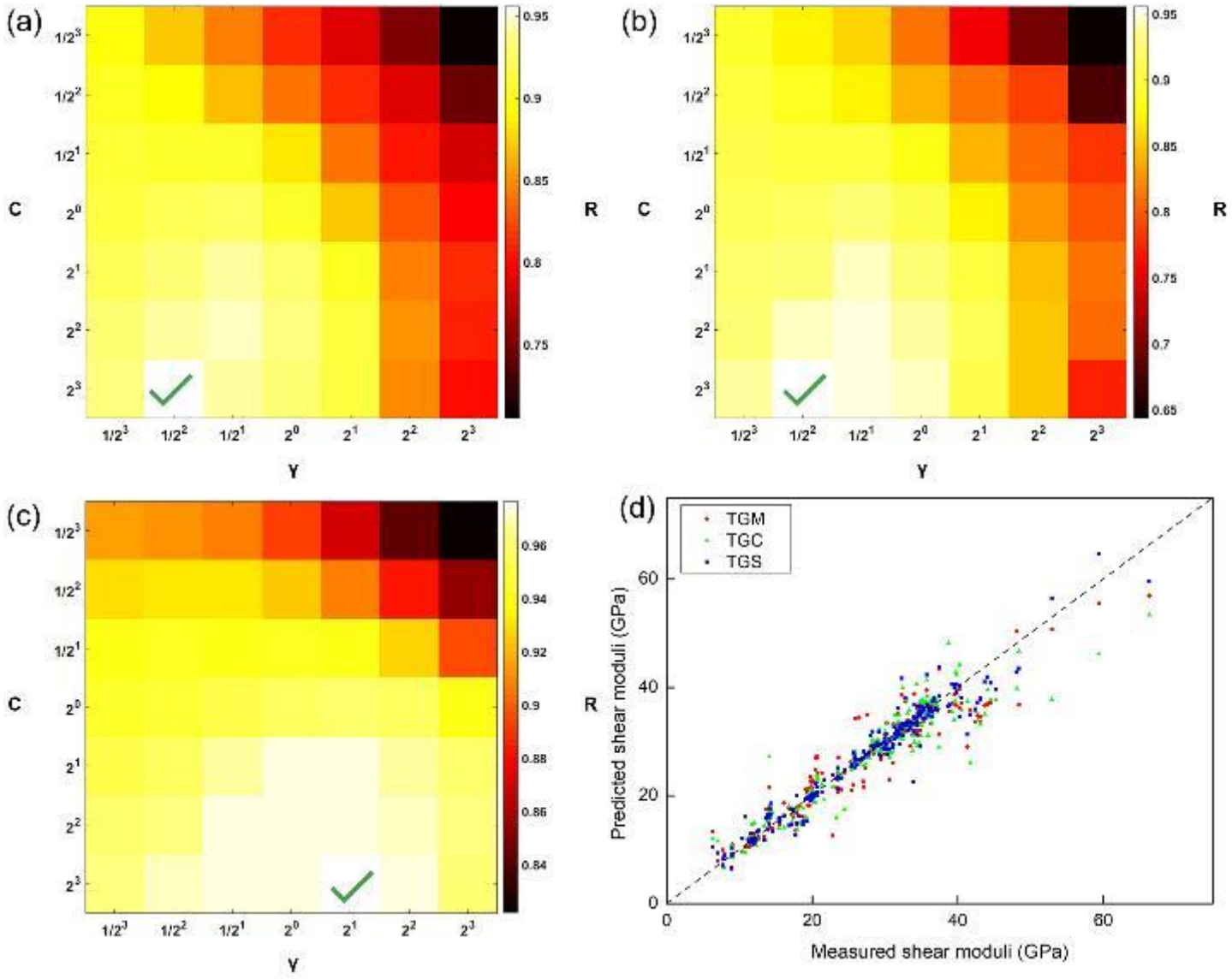

Figure 3. The performance of the SVR-RBF models on the training datasets. *R* of SVR-RBF model is found to have the maximum value of (a) 0.9533 when C=8, γ=0.25 on TGM, (b) 0.9534 when C=8, γ=0.25 on TGC, (c) 0.9742 when C=8 and γ=2 on TGS. (d) The comparing of the predicted *G* with the measured data.

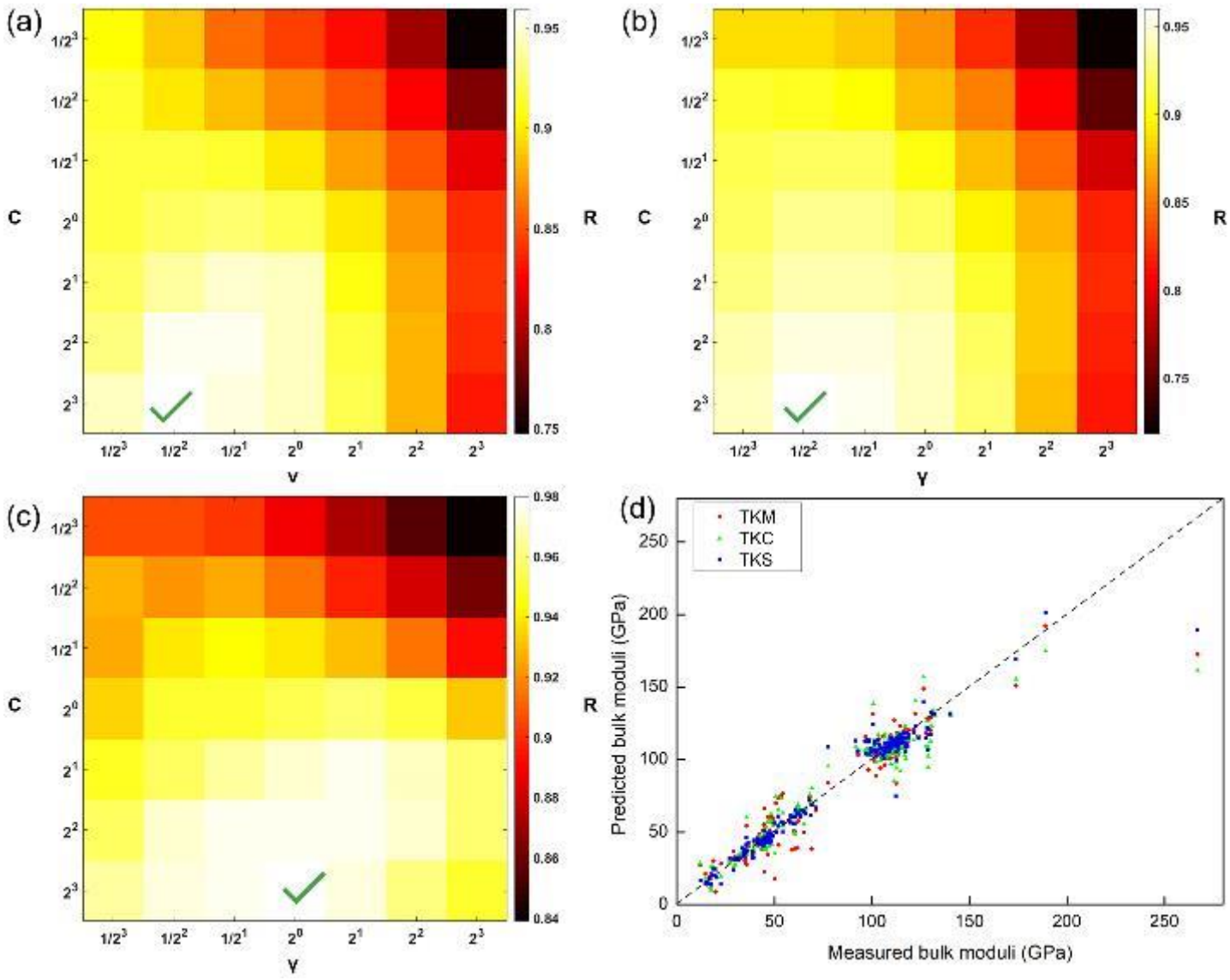

Figure 4. The performance of the SVR-RBF models on the training datasets. *R* of SVR-RBF model is found to have the maximum value of (a) 0.9596 when *C*=8 and *γ*=0.25 on TKM, (b) 0.9581 when *C*=8, *γ*=0.25 on TKC, (c) 0.9779 when *C*=8, *γ*=1 on TKS. (d) The comparing of the predicted *K* with the measured data.

Table 3. The result of grid search on SVR-RBF models

Training set	maximum *R*	*C*	*γ*	*RMSE*
TGM	0.9533	8	0.25	3.2564
TGC	0.9534	8	0.25	3.2545
TGS	0.9742	8	2	2.4252
TKM	0.9896	8	0.25	11.1283
TKC	0.9581	8	0.25	11.3871
TKS	0.9779	8	1	8.2898

Final ML models

To further generalize the SVR models, Pearson VII Universal Kernel (PUK) [31] was applied as a universal kernel function. The PUK function has excellent flexibility by adapting its parameters [29]: penalty parameter (C), kernel parameters (σ and ω). The R-value of SVR-PUK-TGS model has the maximum value of 0.9799 when C=8, σ =8, ω = 0.125 (marked with the green check in Figure 5a), and the maximum value of 0.9791 for the SVR-PUK-KGCa model 0.9791 when C=4, σ =4, ω =0.5 (marked with the green check in Figure 5b).

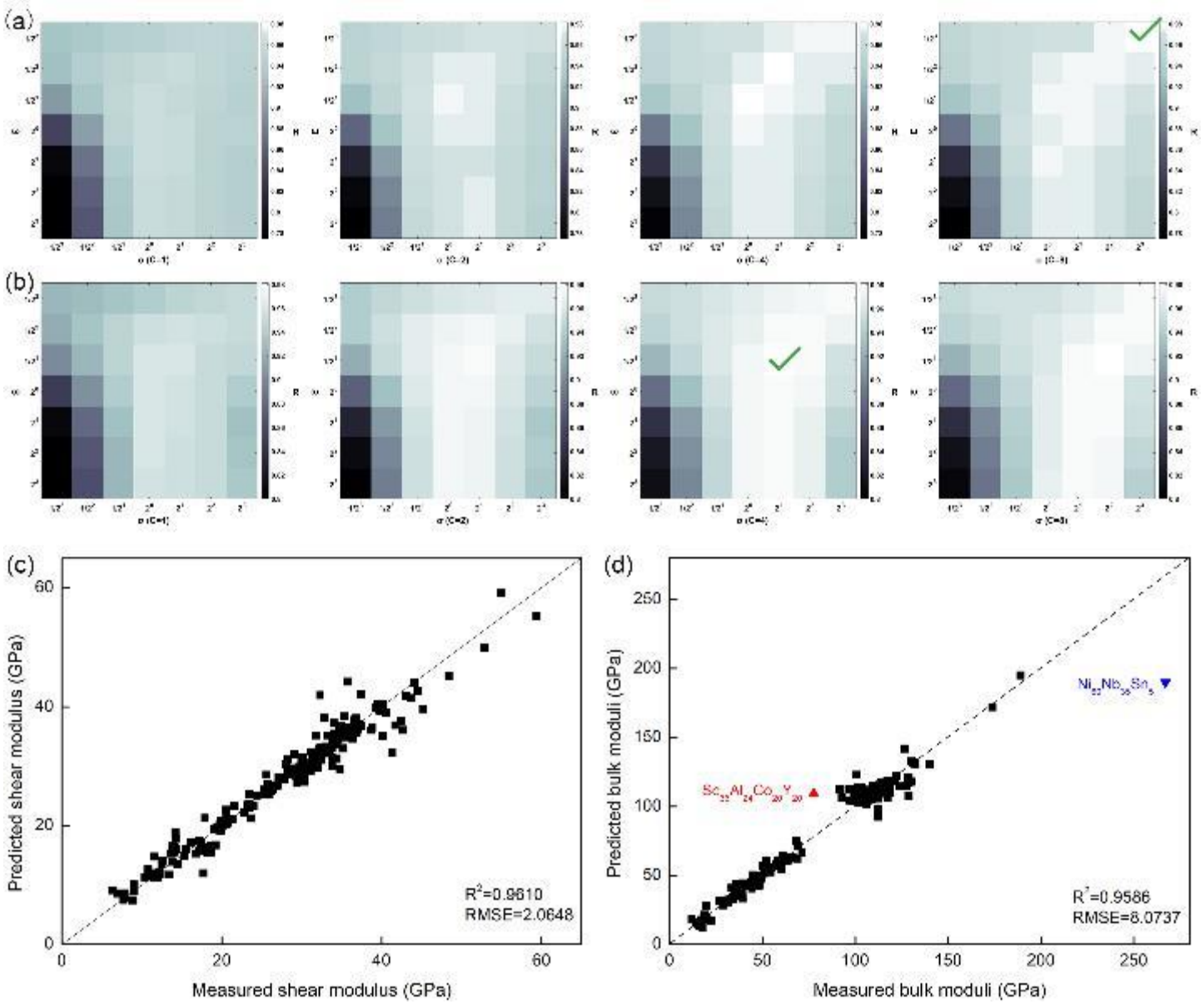

Figure 5. The performance of the SVR-PUK models on the training datasets. R of SVR-PUK model is found to have the maximum value of (a) 0.9799 when C=8, σ =8, ω = 0.125 on TGCa, (b) 0.9791 when C=4, σ =4, ω =0.5 on TGS. (c) SVR-PUK-TGS model predicted G against measured modulus, and (d) SVR-PUK-TKS model predicted K against measured modulus.

Figures 5(c, d) show, respectively, the predicted G and K against the measured values, indicating excellent agreement, as evidenced by R^2>0.958 for both cases. There are a few exceptions, e.g., the bulk moduli of $Sc_{36}Al_{24}Co_{20}Y_{20}$ (red point in Figure 5d) and $Ni_{60}Nb_{35}Sn_5$ (blue point in Figure 5d).

The $Sc_{36}Al_{24}Co_{20}Y_{20}$ is an outlier from the rest of the dataset, only one Sc-based BMG was collected in the dataset, as well as its bulk moduli (only one exists between 75 *GPa* and 90 *GPa*). The blue point in Figure 4d indicates that for $Ni_{60}Nb_{35}Sn_5$, the predicted bulk moduli (189.9 *GPa*) is much lower than the measured (267 *GPa*) [33]. This can be explained by the much lower bulk modulus of the alloy with similar composition in the dataset. 189 *GPa* of $Ni_{60}Sn_6(Nb_{0.8}Ta_{0.2})_{34}$.

Ultrasonic-wave-propagation methods were performed on glassy $Ni_{60}Nb_{35}Sn_5$ to measure the acoustic properties by Haein [34]. The longitudinal propagation velocity C_l was 5.45 *km/s* and transverse propagation velocity C_t was 2.51 *km/s*. The elastic modulus of isotropic materials can be calculated using following equations: (1) $x = \left(\frac{C_l}{C_t}\right)^2$, (2) $\nu = \frac{2-x}{2-2x}$, (3) $G = \rho C_t^2$, (4) $K = \frac{2G(1+\nu)}{3(1-2\nu)}$, where ν is Poisson ratio and ρ is density (8.64g/cm^3 [1] for $Ni_{60}Nb_{35}Sn_5$). The resulting bulk modulus based on acoustic measurements is 183.3 *GPa*, which is very close to our prediction of 189.9 *GPa*. The UWP method also performed on crystalline $Ni_{60}Nb_{35}Sn_5$, the resulting bulk modulus is 152.2 GPa which is much smaller than our prediction

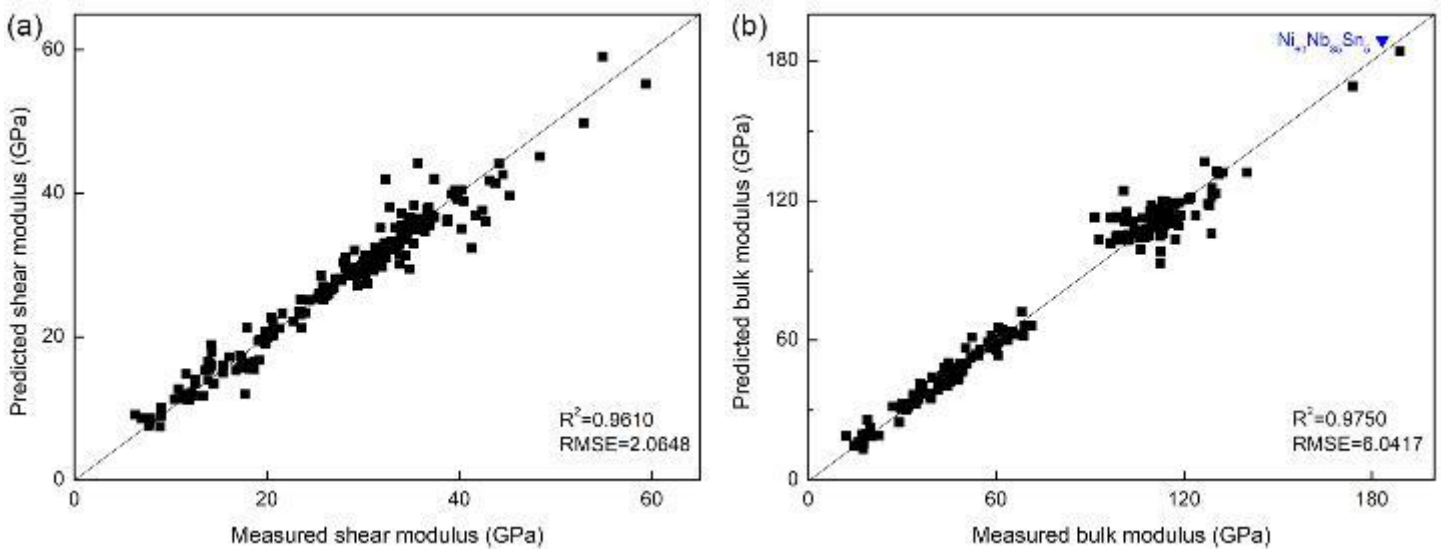

Figure 6. Predicted modulus against updated measured modulus. (c) SVR-PUK-TGS model predicted *G*, and (d) SVR-PUK-TKS model

predicted *K*.

With the updated elastic modulus for $Ni_{60}Nb_{35}Sn_5$, we have retrained ML models and the results are shown in Figure 6. The predicted bulk moduli of 188.7 *GPa* for $Ni_{60}Nb_{35}Sn_5$ is very similar to the updated value, and the final ML models perform much better, as evidenced by improved R^2 for both cases.

Critical casting diameter model

In the development of new BMGs, another issue is to find a relatively universal model to assess the glass forming ability (GFA). The most reliable and quantifiable GFA indicator of an alloy can be the critical cooling rate (R_c). However, it is very difficult to obtain the value of R_c experimentally. A slightly less direct parameter which is the critical casting thickness/diameter (D_{max}) was considered in this research. In general, the larger the Dmax, the higher the GFA should be.

The characteristic temperatures (CTs), T_g (the glass transition temperature), T_x (onset crystallization temperature) and T_l (liquidus temperature), play important roles in the prediction of GFA. Various of GFA criteria have been proposed by investigators based on the functional relationships among CTs in recent decades. Twenty GFA criteria which presented as the mathematical formulas combining the CTs was estimated in this research. And the Matlab 2018 software was used to analyze the correlations between chosen criteria and D_{max}.

The result in table 4 shows the Dmax-criteria correlations. The highest R values is observed as 0.5635 for γ_c criteria, followed by 0.5614 for γ_m criteria. These two criteria were developed based on $\frac{T_x}{T_l}$ and $\frac{T_x-T_g}{T_l}$. Thus, we developed a new parameter γ_n ($\frac{AT_x-BT_g}{T_l}$)) with the D_{max} dataset. And A, B were found to be 5 and 3 in this research with a higher R value (0.5655). The Fitting of best two GFA criteria and new γ_n criteria were shown in figure 7.

In addition, ML models were built for the prediction of D_{max} with the CTs. The ML model based on the Gaussian Process (GP) algorithm with EF kernel show the best performance (R=0.7550), and much better than these developed criteria. The parameters of GP model were estimated by Matlab 2018 as $\sigma_n = 4.6$, $\sigma_f = 5.4$ and $\sigma_l = 0.4$

The performance of GP model is shown in figure 7d. The GP model shows a similar performance with γ_n criteria for small-D_{max} BMGs, but performs much better than γ_n criteria on bigger-D_{max} BMGs.

Table 4. The GFA criteria used in this research, their mathematical formulas, proposed year and investigators. And the values of R for linear correlation between these criteria and D_{max}.

Parameter	Formula	Year	Proposed by	R
ΔT_x	$T_x - T_g$	1991	Inoue A	0.5163
T_{rg}	$\frac{T_g}{T_l}$	2000	Lu ZP	0.3303
γ	$\frac{T_x}{T_g + T_l}$	2002	Lu ZP	0.5446
ΔT_{rg}	$\frac{T_x - T_g}{T_l - T_g}$	2004	Xiao XS	0.5371
α	$\frac{T_x}{T_l}$	2005	Mongal K	0.5077
β_M	$\frac{T_x}{T_g} + \frac{T_g}{T_l}$	2005	Mongal K	0.5498
δ	$\frac{T_x}{T_l - T_g}$	2005	Chen QJ	0.4292
γ_m	$\frac{2T_x - T_g}{T_l}$	2007	Du XH	0.5614
φ	$T_{rg}\left(\frac{\Delta T_x}{T_g}\right)^{0.143}$	.2007	Fan GJ	0.5543
ξ	$\frac{T_g}{T_l} + \frac{\Delta T_x}{T_x}$	2008	Du XH	0.5442
β_Y	$\frac{T_x T_g}{(T_l - T_x)^2}$	2008	Yuan ZZ	0.5199
$\frac{1}{\omega_L}$	$\omega_L = \frac{T_g}{T_x} - \frac{2T_g}{T_g + T_l}$	2009	Long ZL	0.4707
ω_J	$\frac{T_l(T_l + T_x)}{T_x(T_l - T_x)}$	2009	Ji XL	0.4963
θ	$\frac{T_x + T_g}{T_l} \cdot \left(\frac{T_x - T_g}{T_l}\right)^{0.0728}$	2009	Zhang GH	0.4514
ω_A	$\frac{T_g}{2T_x - T_g} - \frac{T_g}{T_l}$	2009	An LX	0.5526
γ_c	$\frac{3T_x - 2T_g}{T_l}$	2010	Guo S	0.5635
β′	$\frac{T_g}{T_x} - \frac{T_g}{1.3T_l}$	2011	Dong BS	0.5540
ω_B	$\frac{2T_x - T_g}{T_l + T_x}$	2015	Blyskum P	0.5564
G_p	$\frac{T_g(T_x - T_g)}{(T_l - T_x)^2}$	2016	Tripathi MK	0.5609

χ	$\frac{T_x - T_g}{T_l - T_x} \cdot \left(\frac{T_x}{T_l - T_x}\right)^{1.47}$	2018	Long ZL	0.5171
γ_n	$\frac{5T_x - 3T_g}{T_l}$	2018	This work	0.5655

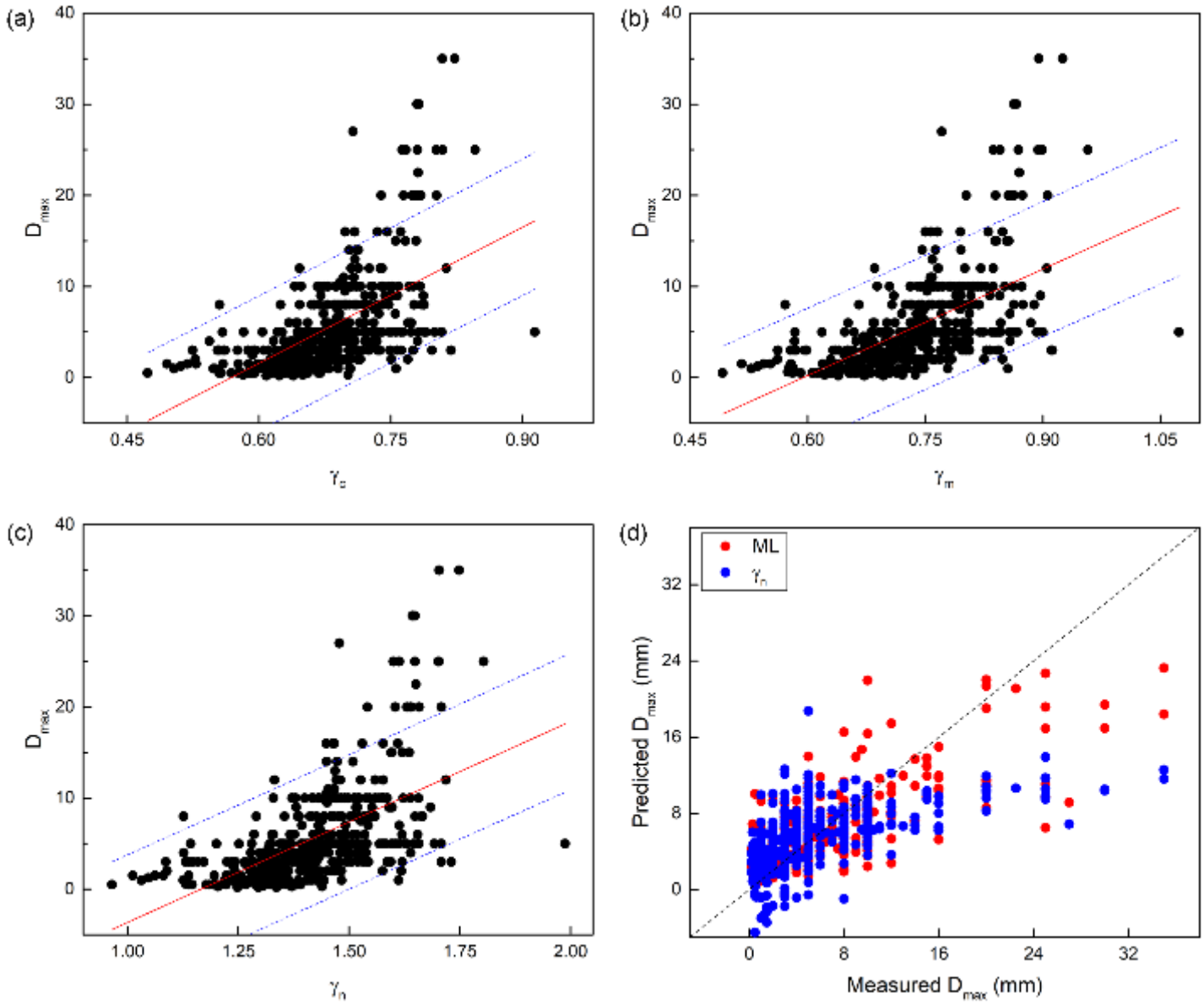

Figure 7. D_{max} vs (a) γ_c (b) γ_m and (c) γ_n criteria in 442 kinds of metal-metal BMGs. (d) The comparing of the predicted D_{max} of GP model (red dots) and γ_n criteria (blue dots) with the measured data.

Conclusions

Machine learning was used to predict the elastic moduli and glass forming ability of metal-metal BMGs. The results show that the best type of atomic radius used in the ML models is the statistical radius. The best subset of features are absolute electronegativity, atomic volume, and atomic size difference. The best ML algorithm is SVR

with PUK function with C=8, σ =8, ω = 0.125 for G, and C=4, σ =2, ω =0.5 for K. GP with EXP function with $\sigma_n = 4.6,\ \sigma_f = 5.4$ and $\sigma_l = 0.4$ for $D_{\max}$

This work indicates the great potential of ML in advanced materials design with target properties.

Acknowledgments

The present research is supported by the PolyU internal grants (No. 1-ZE8R and No. G-YBDH), NSFC (No. 51271157), the research grants (No. 15DZ2260300 and No. 16DZ2260600) from the Science and Technology Commission of Shanghai Municipality, and the 111 Project (No. D16002) from the State Administration of Foreign Experts Affairs and the Ministry of Education, PRC.

References:

[1] W.H. Wang, The elastic properties, elastic models and elastic perspectives of metallic glasses, Prog. Mater. Sci. 57 (2012) 487–656. doi:10.1016/j.pmatsci.2011.07.001.

[2] W. Klement, R.H. Willens, P. Duwez, Non-crystalline structure in solidified Gold-Silicon alloys, Nature. 187 (1960) 869–870. doi:10.1038/187869b0.

[3] R. Ramprasad, R. Batra, G. Pilania, A. Mannodi-Kanakkithodi, C. Kim, Machine learning in materials informatics: Recent applications and prospects, Npj Comput. Mater. 3 (2017). doi:10.1038/s41524-017-0056-5.

[4] S. Ramakrishna, T.Y. Zhang, W.C. Lu, Q. Qian, J.S.C. Low, J.H.R. Yune, D.Z.L. Tan, S. Bressan, S. Sanvito, S.R. Kalidindi, Materials informatics, J. Intell. Manuf. (2018) 1–20. doi:10.1007/s10845-018-1392-0.

[5] A. Agrawal, A. Choudhary, Perspective: Materials informatics and big data: Realization of the “fourth paradigm” of science in materials science, APL Mater. 4 (2016). doi:10.1063/1.4946894.

[6] T. Mueller, A.G. Kusne, R. Ramprasad, Machine Learning in Materials Science, Rev. Comput. Chem. 29 (2016) 186–273. doi:10.1002/9781119148739.ch4.

[7] M.L. Green, C.L. Choi, J.R. Hattrick-Simpers, A.M. Joshi, I. Takeuchi, S.C. Barron, E. Campo, T. Chiang, S. Empedocles, J.M. Gregoire, A.G. Kusne, J. Martin, A. Mehta, K. Persson, Z. Trautt, J. Van Duren, A. Zakutayev, Fulfilling the promise of the materials genome initiative with high-throughput experimental methodologies, Appl. Phys. Rev. 4 (2017). doi:10.1063/1.4977487.

[8] Y.T. Sun, H.Y. Bai, M.Z. Li, W.H. Wang, Machine Learning Approach for Prediction and Understanding of Glass-Forming Ability, J. Phys. Chem. Lett. 8 (2017) 3434–3439. doi:10.1021/acs.jpclett.7b01046.

[9] Z.Q. Liu, Z.F. Zhang, Strengthening and toughening metallic glasses: The elastic perspectives and opportunities, J. Appl. Phys. 115 (2014). doi:10.1063/1.4872249.

[10] L.D. Landau, E.M. Lifshitz, Theory of Elasticity 3rd edition, 1986.

[11] IUPAC, Compendium of Chemical Terminology, 2014. doi:10.1351/goldbook.I03352.

[12] J.Q. Wang, W.H. Wang, H.B. Yu, H.Y. Bai, Correlations between elastic moduli and molar volume in metallic glasses, Appl. Phys. Lett. 94 (2009). doi:10.1063/1.3106110.

[13] K. Zhao, Z. Bai, L. Zhang, G. Liu, Correlation between atomic size and elastic properties/glass transition temperature in metallic glasses, Sci. China Physics, Mech. Astron. 60 (2017). doi:10.1007/s11433-017-9053-9.

[14] M.X. Xia, Q.G. Meng, S.G. Zhang, C.L. Ma, J.G. Li, Thermodynamic characteristics of metallic glass-forming liquids, Acta Phys. Sin. 55 (2006) 6543–6549.

[15] Q. Jiang, B.Q. Chi, J.C. Li, A valence electron concentration criterion for glass-formation ability of metallic liquids, Appl. Phys. Lett. 82 (2003) 2984–2986. doi:10.1063/1.1571984.

[16] A. Stolcke, S. Kajarekar, L. Ferrer, Nonparametric feature normalization for SVM-based speaker verification, in: ICASSP, IEEE Int. Conf. Acoust. Speech Signal Process. - Proc., 2008: pp. 1577–1580. doi:10.1109/ICASSP.2008.4517925.

[17] A. Inoue, A. Takeuchi, Recent development and application products of bulk glassy alloys, Acta Mater. 59 (2011) 2243–2267. doi:10.1016/j.actamat.2010.11.027.

[18] K.J. Laws, D.B. Miracle, M. Ferry, A predictive structural model for bulk metallic glasses, Nat. Commun. 6 (2015). doi:10.1038/ncomms9123.

[19] H. Peng, S.S. Li, T.Y. Huang, A glass forming ability indicator of mg-based metallic glasses using atomic radius and electronegativity. Journal of Tsinghua University, 8(2010), 1188-1192.

[20] Z.P. Lu, C.T. Liu, Y.D. Dong, Effects of atomic bonding nature and size mismatch on thermal stability and glass-forming ability of bulk metallic glasses, J. Non. Cryst. Solids. 341 (2004) 93–100. doi:10.1016/j.jnoncrysol.2004.04.024.

[21] P. Pyykkö, M. Atsumi, Molecular single-bond covalent radii for elements 1-118, Chem. - A Eur. J. 15 (2009) 186–197. doi:10.1002/chem.200800987.

[22] D.B. Miracle, A physical model for metallic glass structures: An introduction and update, JOM. 64 (2012) 846–855. doi:10.1007/s11837-012-0359-4.

[23] B. Cordero, V. Gómez, A.E. Platero-Prats, M. Revés, J. Echeverría, E. Cremades, F. Barragán, S. Alvarez, Covalent radii revisited, J. Chem. Soc. Dalt. Trans. (2008) 2832–2838. doi:10.1039/b801115j.

[24] D. Mladenic, Feature selection for dimensionality reduction, Subspace, Latent Struct. Featur. Sel., 2006: pp. 84–102. doi:10.1007/11752790_5.

[25] G. James, D. Witten, R. Tibshirani, T. Hastie, An Introduction to Statistical Learning with Applications in R, 2013.

[26] J.E. Huheey, E. a. Keiter, R.L. Keiter, Inorganic Chemistry: Principles of Structure and Reactivity (4th Edition), Inorg. Chem. Princ. Struct. React. (1993) 513–515. doi:10.1007/SpringerReference_9061.

[27] P. Bouboulis, S. Theodoridis, C. Mavroforakis, L. Evaggelatou-Dalla, Complex support vector machines for regression and quaternary classification, IEEE Trans. Neural Networks Learn. Syst. 26 (2015) 1260–1274. doi:10.1109/TNNLS.2014.2336679.

[28] R.G. Brereton, G.R. Lloyd, Support Vector Machines for classification and regression, Analyst. 135 (2010) 230–267. doi:10.1039/B918972F.

[29] P. Machine, L. Tools, I.H. Witten, E. Frank, Data mining: practical machine learning tools and techniques with Java implementations, 2002. doi:10.1145/507338.507355.

[30] D. Xue, D. Xue, R. Yuan, Y. Zhou, P. V. Balachandran, X. Ding, J. Sun, T. Lookman, An informatics approach to transformation temperatures of NiTi-based shape memory alloys, Acta Mater. 125 (2017) 532–541. doi:10.1016/j.actamat.2016.12.009.

[31] G. Zhang, H. Ge, Support vector machine with a Pearson VII function kernel for discriminating halophilic and non-halophilic proteins, Comput. Biol. Chem. 46 (2013) 16–22. doi:10.1016/j.compbiolchem.2013.05.001.

[32] X.K. Xi, S. Li, R.J. Wang, D.Q. Zhao, M.X. Pan, W.H. Wang, Bulk scandium-based metallic glasses, J. Mater. Res. 20 (2005) 2243–2247. doi:10.1557/JMR.2005.0281.

[33] H. Choi-Yim, D. Xu, W.L. Johnson, Ni-based bulk metallic glass formation in the Ni–Nb–Sn and Ni–Nb–Sn–X (X=B,Fe,Cu) alloy systems, Appl. Phys. Lett. 82 (2003) 1030–1032. doi:10.1063/1.1544434.

[34] H. Choi-Yim, D. Xu, M.L. Lind, J.F. Löffler, W.L. Johnson, Structure and mechanical properties of bulk glass-forming Ni-Nb-Sn alloys, Scr. Mater. 54 (2006) 187–190. doi:10.1016/j.scriptamat.2005.09.040.

[35] W. Jiao, D.Q. Zhao, D.W. Ding, H. Bai, W.H. Wang, Effect of free electron concentration on glass-forming ability of Ca-Mg-Cu system, J. Non. Cryst. Solids. 358 (2012) 711–714. doi:10.1016/j.jnoncrysol.2011.10.033.

[36] S. Zhao, J.H. Li, S.M. An, S.N. Li, B.X. Liu, Computational assisted design of the favored composition for metallic glass formation in a Ca-Mg-Cu system, RSC Adv. 7 (2017) 39082–39088. doi:10.1039/c7ra05650h.